Investigation on Rotation Response of Spin-Exchange Relaxation-Free Atomic Spin Gyroscope

YUANHONG YANG[1], **DONGYING CHEN**[1], **WEI JIN**[2], **WEI QUAN**[1,3], **FENG LIU**[1], **AND JIANCHENG FANG**[1,3]

[1]School of Instrumentation and Optoelectronic Engineering, Beihang University, Beijing 100191, China
[2]Department of Electrical Engineering, The Hong Kong Polytechnic University, Hong Kong
[3]Science and Technology on Inertial Laboratory, Beihang University, Beijing 100191, China

Corresponding authors: Yuanhong Yang (yhyang@buaa.edu.cn) and Wei Jin (eewjin@polyu.edu.hk)

ABSTRACT Spin-exchange relaxation-free atomic spin gyroscope (SERF gyro) has ultrahigh theoretical sensitivity and is regarded as one of the most potential atomic gyroscopes. To investigate its rotation response, a high linear atomic spin precession detection module was developed firstly by modifying the fiber reflective Sagnac interferometer for atomic spin precession detection and operating it in closed-loop mode. The SERF gyro based on K-Rb-^{21}Ne comagnetometer was built and tested and appeared obvious nonlinear response feature. The nonlinear rotation response model was deduced by assuming the rotation-induced nuclei spin procession detecting as an *in-situ* magnetometer inside the SERF gyro and the fitting curves are in good agreement with the experimental results. The optimized pump power for maximum sensitivity and measurable dynamic range were analyzed theoretically and demonstrated experimentally. The investigation results show that the nonlinear rotation response is an intrinsic property of SERF gyro and its measurable dynamic range is limited due to the saturation characteristic of the sum of pumping and relaxation rate. This indicates that SERF gyro is propitious to a position gyroscope with high sensitivity.

INDEX TERMS Atomic spin gyroscope, spin-exchange relaxation-free, nonlinear rotation response model, atomic spin precession detection.

I. INTRODUCTION

Gyroscopes are considered as core components of the inertial system which play an important role in the inertial navigation system [1]–[3]. In recent years, atomic gyroscopes have attracted extensive attention due to their ultrahigh sensitivity, high precision and miniaturized structure [4], [5]. Spin-exchange relaxation-free atomic spin gyroscope (SERF gyro) which was first demonstrated in 2005 by Kornack *et. al* [6] has ultrahigh theoretical sensitivity and is regarded as one of the most potential atomic gyroscopes now. A bias instability of 0.009 deg/h was achieved by using a train of ^{87}Rb π pulses and $\sigma+/\sigma-$ optical pumping technology [7] and a dual-axis SERF gyro using the parametric modulation

technique was demonstrated and a rotation sensitivity of 1.093×10^{-6} rad/s/Hz$^{1/2}$ was reported [8]. Up to now, most studies on SERF gyro have focused on the bias instability and rotation sensitivity based on the linear model demonstrated in [6]. However, as key performance parameters, its dynamic range and scale factor linearity have not attracted sufficient attention and the rotation response of SERF gyro has not been specially investigated. In this paper, we experimentally and theoretically investigated the rotation response of SERF gyro.

In SERF gyro, it is significant to detect precisely and linearly the atomic spin precession due to rotation. The conventional detection method is based on the classical Malus's Law by using an off-resonance laser with a well-defined linear polarization and analyzing its polarization state after passing through the vapor [9]–[11]. And the high precision has been obtained based on the differential polarization detection
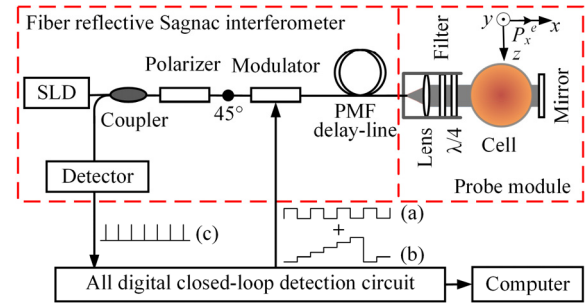
The associate editor coordinating the review of this manuscript and approving it for publication was Chao Zuo.

and modulation technology, etc. [12]–[15]. However, there are some drawbacks, such as limited linear measurement range, bulky optical configuration, sensitive to thermal and vibrations fluctuations, etc.. Recently, our group proposed and experimentally demonstrated a single-fiber Sagnac-like interferometer for atomic spin precession detection with two oppositely circularly polarized beams instead of linear polarized light. The open-loop detection system has been first constructed and successfully demonstrated in a SERF magnetometer [16]. In this paper, we improved the detection system further and operated it in closed-loop mode with excellent linearity in large measure range. Based on this technology, the rotation response of a SERF gyro was investigated successfully. In section II, the linear atomic spin precession detection module was proposed and developed by modifying the closed-loop fiber reflective Sagnac interferometer and let it operate in closed-loop mode. Its construct modification and operation principle were described and demonstrated briefly. In section III, the experiment setup of a SERF gyro based on K-Rb-^{21}Ne comagnetometer was built and its rotation response was tested under different pump powers. The experimental results revealed its nonlinear response feature. In section IV, the cooperation condition of the self-compensating K-Rb-^{21}Ne comagnetometer was analyzed in detail and it was found that the nuclei spin precession detecting can be equivalent to an *in-situ* magnetometer inside the SERF gyro. The nonlinear rotation response model was established based on this assumption and the model fitting results agree well with the experimental data. Furthermore, the optimized pump power for maximum sensitivity and measurable dynamic range were analyzed theoretically and demonstrated experimentally. The investigation shows the nonlinear rotation response is an intrinsic property of SERF gyro and it is propitious to a position gyroscope with high sensitivity.

II. LINEAR ATOMIC SPIN PRECESSION DETECTION

Figure 1 shows the linear atomic spin precession detection scheme based on the modified closed-loop fiber optic spin precession detection scheme. It is composed of a fiber reflective Sagnac interferometer, a probe module, and an all-digital closed-loop detection circuit. The fiber reflective Sagnac interferometer is similar with the initial structure proposed in [16], but a broadband superluminescent diode (SLD) is used instead of the narrow linewidth diode laser to reduce the interference noise in the reciprocal optical path. The probe module consists of a collimating lens, an optical spectrum filter, a quarter-wave (λ/4) plate, a vapor cell, and a mirror. Where two circularly polarized probe lights of opposite helicity are taken as the probe lights instead of traditional linearly polarized light. The first three devices are assembled in a lens tube and the mirror is mounted on the opposite side of the vapor cell.

The fiber reflective Sagnac interferometer is a typical polarization mode interferometer and the evolution of polarization modes in the interferometer has been described in

FIGURE 1. Schematic diagram of modified closed-loop fiber reflective Sagnac interferometer for atomic spin precession detection. SLD is superluminescent diode, PMF is polarization-maintaining fiber, Lens is collimating lens. P_x^e is the alkali metal atoms spin polarization component along the x-axis and detected.

detail in [16]. Two polarization modes formed at 45° splice point have traveled along both axes of the polarization-maintaining fiber (PMF) delay-line as right and left circularly polarized lights in the vapor cell only in reverse order. This ensures the interferometer excellent reciprocity and insensitive to environmental disturbances. The only source of phase shift between the two polarization modes is caused in the polarized vapor cell. The interference light intensity detected by the photodetector can be given by,

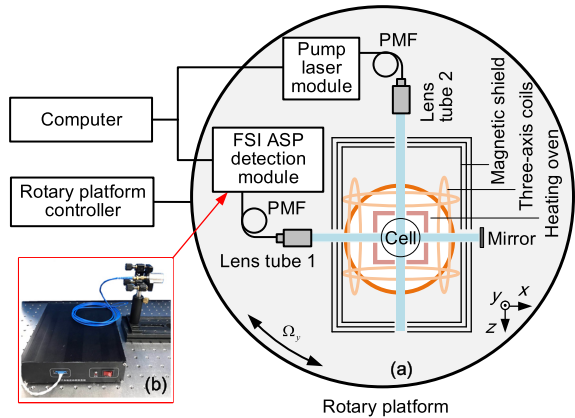$$I_{out}(t) = \frac{1}{2}I_s\eta \ \{1 + \cos[\varphi_m(t) - \varphi_m(t-\tau) + \Delta\varphi]\} \quad (1)$$

where I_s is the source intensity of SLD, η is the optical loss coefficient, τ is the propagation delay time of the two waves passing through the modulator forward and backward. $\varphi_m(t)$ and $\varphi_m(t-\tau)$ represent the modulation phase produced by modulator at time of t and t-τ, respectively. φ is the phase difference between the two circularly polarized probe lights, it is four times the optical rotation angle when the linearly polarized lights were used as probe lights.

Based on the closed-loop fiber optic gyroscope (FOG) technique [17], this interferometer takes a Ti-diffused LiNbO$_3$ integrated optical straight waveguide as birefringence modulation and is operated in closed-loop mode with the all-digital closed-loop detection circuit. The π/2 bias modulation waves (a) and the phase step waves (b) were added on the modulator simultaneously to provide bias modulation and a nonreciprocal phase shift equal and opposite to the phase difference, the first harmonic of the periodic waveform (c) was thereby nulled and the nonreciprocal phase shift was then a measure for φ. The output digital quantity of the closed-loop detection circuit can be written as [9], [17],

$$D = K_D \cdot \Delta\varphi = K_D \cdot K_V \cdot l \cdot P_x^e \quad (2)$$

$$K_V = \frac{\pi}{3}nr_ec \ \{\text{Im}[V(\nu - \nu_{D2})] - \text{Im}[V(\nu - \nu_{D1})]\} \quad (3)$$

where K_D is the conversion coefficient from the phase difference φ to the output digital quantity. K_V is the equivalent Wilder coefficient of the polarized vapor cell. l is the propagation distance of light in the vapor cell. P_x^e is the alkali-metal atoms spin polarization component along the x axis,
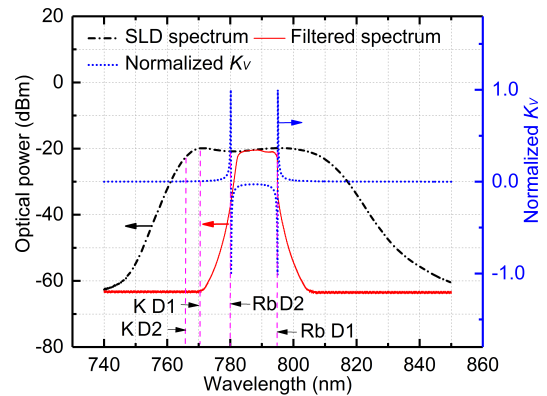
FIGURE 2. (a) Experimental setup diagram of SERF gyro. The pump laser module contained an ECDL laser, an amplifier, and their driver. FSI ASP detection module is the integrated closed-loop fiber reflective Sagnac interferometer for atomic spin precession detection. The lens tube 1 contained a collimator, a filter, and a λ/4 plate, the lens tube 2 contained a collimator and a λ/4 plate. (b) Photograph of the FSI ASP detection module.

FIGURE 3. SLD spectrum, filtered spectrum and normalized curve of K_V.

as shown in Fig. 1. n is the density of alkali-metal atoms, r_e is the electron radius of the alkali-metal atom, c is the velocity of light in vacuum, ν is the light frequency, ν_{D1} and ν_{D2} are the resonance frequency of D1 and D2 line of alkali-metal atoms, respectively. $\text{Im}[V(\nu\text{-}\nu_{D1})]$ and $\text{Im}[V(\nu\text{-}\nu_{D2})]$ represent the imaginary part of the Voigt profile of resonance frequency ν_{D1} and ν_{D2}, respectively. As described in (2) and (3), the P_x^e can be measured linearly and accurately within a large phase difference range without any approximation. Thanks to mature closed-loop FOG technology, the excellent linearity of less than 10^{-6} and high phase resolution of less than 10^{-8} rad can be achieved [17] in this linear atomic spin precession detection system.

III. EXPERIMENTAL SETUP AND RESULTS

Figure 2(a) shows the schematic illustration of the experimental setup of the SERF gyro based on K-Rb-^{21}Ne comagnetometer. The core unit was a 15 mm diameter spherical cell made from GE180 aluminosilicate glass. The cell contained a mixture of K, Rb (72.2% ^{85}Rb and 27.8% ^{87}Rb) alkali-metals, 2.7 atm of ^{21}Ne gas and 50 torr of N_2 gas for quenching, the density ratio of K to Rb atoms was about 1:100. The cell was mounted in a boron nitride ceramic shell frame and heated to ~185 °C by a non-magnetic electric heater driven by a 50 kHz AC source. A set of three orthogonal Helmholtz coils was driven independently by three high current function generators (Keithley Model 6221) to zero the magnetic field at the location of the vapor cell. All the components above were mounted inside the three-layer μ-metal magnetic shields with a shielding factor of 10^5. The pump laser module contained a 770.1 nm (K atom D1 line) ECDL laser, a tapered amplifier, and their driver. The lens tube 2 contained a collimator and a λ/4 plate. The amplified pump laser was led through PMF to the lens tube 2 and circularly polarized by the λ/4 plate. In the K-Rb-^{21}Ne comagnetometer, the function of optically pumped K atoms is to polarize Rb atoms while the polarized Rb atoms are used not only to hyperpolarize ^{21}Ne
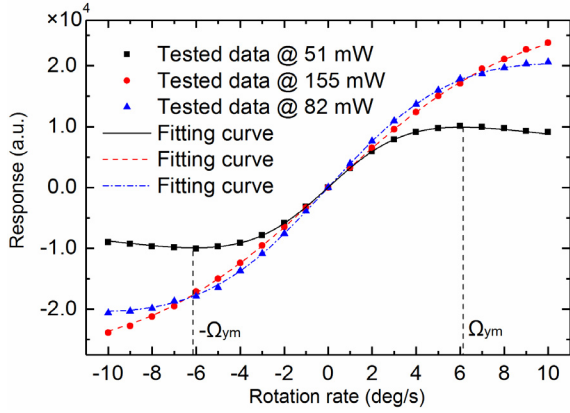
nuclei but also to sense the spin procession due to the applied rotation rate.

The fiber reflective Sagnac interferometer and all-digital closed-loop detection circuit shown in Fig. 1 were integrated to form the closed-loop fiber reflective Sagnac interferometer for atomic spin precession detection (abbreviated as FSI ASP detection module) and packaged in an instrument box with the size of 22 cm × 17 cm × 6 cm. The photograph of the FSI ASP detection module is shown in Fig. 2(b). The mirror, vapor cell and lens tube 1 containing a collimator, a filter and a λ/4 plate constituted the probe module. As shown in Fig. 2 (a), the FSI ASP detection module, the pump laser module, and the probe module were all mounted on a rotary platform and the y-axis of the SERF gyro was parallelly aligned to the rotation axis of the rotary platform. The K atoms in vapor cell were polarized along the z-axis and the Rb atoms electron spin polarization component P_x^e along the x-axis was detected by the FSI ASP detection module and the output was recorded by a computer.

To reduce the interference noise due to stray reflection light of optical components and parasitic interference in fibers, the broadband SLD with the mean wavelength of 787 nm and bandwidth of 43 nm was used as the light source and its spectrum is shown in Fig. 3. The normalized K_V was simulated based on (3) with the typical parameters listed in [9] and shown in Fig. 3. It can be seen the spectrum width of SLD is larger than the space between Rb D1 and D2 lines and the wavelength dependence K_V has reverse values at the left and right of the Rb D1 (and D2) line. This results in smaller output because the output is proportional to the integral value over the source spectrum bandwidth. To guarantee high sensitivity, a specially designed band-pass optical filter was inserted before the λ/4 plate. The filtered spectrum is shown in Fig. 3 and covers almost the spectrum space between Rb D1 and D2 lines. Therefore, high sensitivity and low interference noise were satisfied simultaneously.

During the experiment, the residual magnetic fields in the volume of the K-Rb-^{21}Ne vapor cell was compensated firstly with the *in-situ* triaxial magnetic field compensation technique by analyzing the pump light intensity transmitted through the cell [18], and the residual magnetic field of less
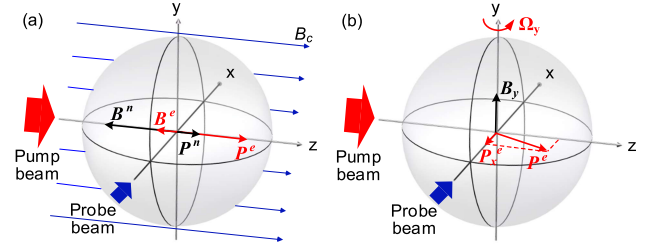
FIGURE 4. Rotation response of SERF gyro under different pump powers. The tested data are fitted to the nonlinear rotation response model proposed below. The maximum sensitivity curve was shown at an optimized pump power of 82 mW.

than 2 nT was achieved. The SERF gyro is operated in the SERF regime and the special cooperation condition, i.e. $B_c = -(B^n + B^e)$ must be satisfied, as shown in Fig. 5 (a), where B_c is the applied bias magnetic field parallel to the pump beam (z-axis), B^n and B^e are created by the nuclear and electron magnetization respectively along the z-axis. For this purpose, the procedure of magnetic field B_z compensating was carried out and the zero compensating point was identified based on the response to a B_y modulation square wave at various B_c values and the compensation value of B_c was set accurately [19]. Under the SERF regime and self-compensation condition, we tested the gyroscopic rotation response from -10.0 deg/s to $+10.0$ deg/s with an interval of 1 deg/s under different pump powers of 51 mW and 155 mW preliminarily. The tested data were shown in Fig. 4 and appeared typical Lorentzian dispersion feature, i.e. obvious nonlinearity within the applied rotation rate range. Besides, the measurable monotone range is smaller and closely related to the pump power. In our previous work, this similar phenomenon has been observed in the parametrically modulated dual-axis atomic spin gyroscope [8] and the investigation on the real-time closed-loop control of the compensation point in the K-Rb-^{21}Ne comagnetometer [20] and can confirm these tested results further.

At the rotation rate of ±10.0 deg/s, the corresponding phase difference $\Delta\varphi$ between the two circularly polarized lights of opposite helicity is far less than 2π rad and the linearity of the FSI ASP detection module can be well guaranteed because its measurable phase difference range is beyond 2π. Therefore, the observed nonlinear response must be attributed to the intrinsic property of the SERF gyro itself.

IV. ROTATION RESPONSE MODEL
As mentioned above, the SERF gyro is operated in the SERF regime while the special cooperation condition for the self-compensating comagnetometer is satisfied, as shown in Fig. 5(a). Under this cooperation condition, the nuclear magnetization will adiabatically cancel to any first-order fluctuations in the external field along transverse axes and all net

FIGURE 5. The schematic diagram of equivalent *in-situ* Rb atoms magnetometer in SERF gyro. (a) When the special cooperation condition for the self-compensating comagnetometer is satisfied, $B_c = -(B^n + B^e)$, the net magnetic fields along x, y and z axes are all close to zero. (b) When a rotation rate Ω_y is applied (B_c, B^n, B^e, P^n *are not shown*), only the equivalent magnetic field B_y is experienced by the Rb atoms and the component of electron spin polarization P_x^e will be detected.

magnetic field $\mathbf{B}$ and light shift $\mathbf{L}$ can be regarded as zero. The rotation response equation was simplified as following in the early literature [6], [13]:

$$P_x^e = \frac{P_z^e \gamma_e \Omega_y}{\gamma_n R_{tot}} \quad (4)$$

$$R_{tot} = R_P + R_{rel} \quad (5)$$

where $P_z^e = R_p/R_{tot}$ is the equilibrium polarization of the electron along the z- axis, R_p is the pumping rate of the pump beam, R_{tot} is sum of the pumping rate R_p and the relaxation rate R_{rel}. Ω_y is the applied rotation rate along the y-axis. γ_e and γ_n are the gyromagnetic ratio of electron and nuclear spin, respectively. Up to now, most studies on SERF gyro have focused on the bias instability and rotation sensitivity based on this linear model. However, referring to the experimental results shown in Fig. 4, it is found that this linear model may be valid only within a very small rotation rate range and further refinement for large rotation rate range is needed.

In SERF gyro based on K-Rb-^{21}Ne comagnetometer, for example, the polarized Rb atoms are taken to polarize ^{21}Ne atoms and sense the spin procession due to the applied rotation rate. When a rotation rate Ω_y was applied along the y-axis, only the equivalent magnetic field B_y will be experienced by the Rb atoms and the component of electron spin polarization P_x^e will be detected with the FSI ASP detection module, as shown in Fig. 5(b). This procedure can be equivalent to an *in-situ* magnetometer inside the SERF gyro and described with the classical Bloch equation of the electron spins [21]:

$$\frac{\partial \mathbf{P^e}}{\partial t} = \frac{1}{q}\left[\gamma_e \mathbf{B} \times \mathbf{P^e} + R_p\left(\hat{z} - \mathbf{P^e}\right) - R_{rel}\mathbf{P^e}\right] \quad (6)$$

where the pump rate of the probe light is neglected, $\mathbf{P^e}$ is the electron spin polarization vector, $\mathbf{B}$ is the magnetic field experienced by the electrons. When the cooperation condition mentioned above was satisfied and the applied rotation rate is Ω_y, $B_x = 0$, $B_y = \Omega_y/\gamma_n$, and $B_z = 0$, the component of electron spin polarization P_x^e can be solved out as following,

$$P_x^e = \frac{P_z^e \gamma_e \Omega_y}{R_{tot}\gamma_n\left(1 + \left(\frac{\gamma_e}{R_{tot}\gamma_n}\right)^2 \Omega_y^2\right)} \quad (7)$$

TABLE 1. The K_1 and K_2, the calculated values of R_{tot} and Ω_{ym} under different pump powers.

W_p (mW)	K_1 (deg/s)$^{-1}$	K_2 (deg/s)$^{-2}$	R_{tot} (s^{-1})	Ω_{ym} (deg/s)
51	3154	0.0266	891	6.1
155	3341	0.0029	2698	18.5
82	3872	0.0077	1656	11.4

Equation (7) is a typical Lorentzian dispersion response function and the maximum values will be reached at $\pm\Omega_{ym}$ described as following:

$$\Omega_{ym} = \gamma_n R_{tot} / \gamma_e \tag{8}$$

When $\Omega_y << \Omega_{ym}$, the term containing Ω_y^2 can be ignored and (4) can be obtained from (7). This indicates that the linear response model (4) is the special linear form of (7) at a small rotation rate by approximation.

Combining (2) and (7), the rotation rate Ω_y can be expressed in terms of output numerical quantities D which can be rewritten to fit the Lorentzian dispersion function:

$$D = \frac{K_1 \Omega_y}{1 + K_2 \Omega_y^2} \tag{9}$$

$$K_1 = \left(K_D K_V l R_p \gamma_e\right) \Big/ \left(R_{tot}^2 \gamma_n\right) \tag{10}$$

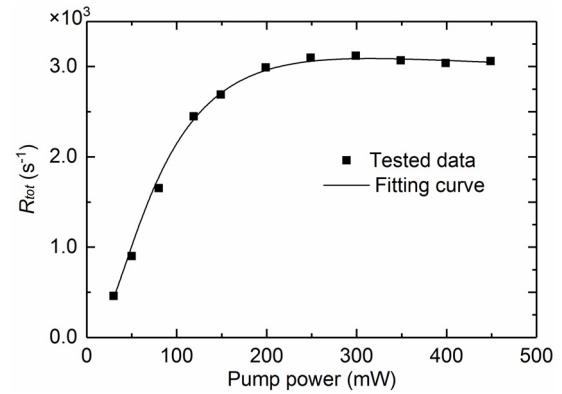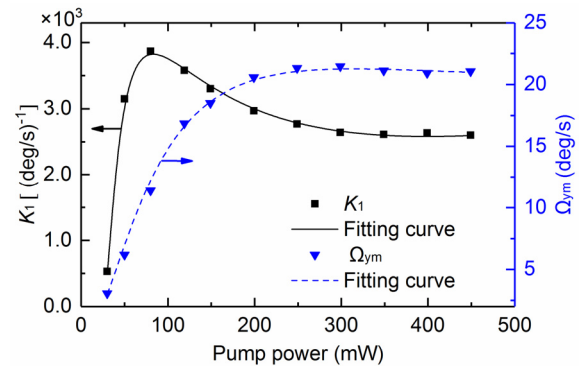$$K_2 = \left(\gamma_e / R_{tot} \gamma_n\right)^2 \tag{11}$$

where K_1 is a comprehensive coefficient related to the polarized vaper cell and the FSI ASP detection module. The coefficient K_2 is inversely proportional to the square of R_{tot}.

The tested data under different pump powers are fitted according to (9) and the fitting curves are plotted in Fig. 4. The R-square values (the goodness of the fit) of the nonlinear fitting are all superior to 0.99, this shows a good agreement between the tested data and the nonlinear rotation response model and proves further that it is reasonable to regard the rotation rate sensing behavior in SERF gyro as an *in-situ* magnetometer which is sensitive only to the equivalent magnetic field produced by inertial rotation. The fitted model parameters are all listed in Table 1. In the SERF gyro based on K-Rb^{-21}Ne comagnetometer, $\gamma_e = 2.80 \times 10^{10}$ Hz/T and $\gamma_n = 3.37 \times 10^6$ Hz/T, the R_{tot} and the rotation rate Ω_{ym} at the maximum response were calculated out according to (11) and (8) and listed in Table 1 too. The experimental and theoretical investigation results both reveal the nonlinear rotation response characteristic of the SERF gyro and its rotation sensitivity and dynamic range are both related closely to R_{tot}.

Substituting (5) to (10), when $R_p = R_{rel}$, we can get the maximum rotation sensitivity as following,

$$K_1 = \left(K_D K_V l \gamma_e\right) \Big/ \left(4 R_p \gamma_n\right) \tag{12}$$

This indicates there must be an optimal pump power to achieve maximum rotation sensitivity for the SERF gyro.

FIGURE 6. The measured R_{tot} and fitting curve. R_{tot} will be saturated when the pump power is bigger than ~250 mW. The fitting curve was obtained by nonlinear fitting in Origin software.

FIGURE 7. Curves of K_1 and Ω_{ym} vs. pump power. The fitting curves were obtained by nonlinear fitting in origin software.

From the equation (8), the SERF gyro measurable maximum rotation rate Ω_{ym} is determined by the R_{tot}. In our previous works [22], we have modeled and demonstrated that the spin-exchange relaxation in K-Rb-^{21}Ne comagnetometer is related closely to spin-exchange interaction between Rb and ^{21}Ne spins and effected closely by the spin polarization of Rb. This will let R_{tot} saturated when the pump power was big enough.

Increasing the pump power, we investigated the evolution characteristic of R_{tot} in the SERF gyro by testing the rotation response at each pump power. The values of R_{tot} were calculated out based on the fitting results according to (9)-(11). The similar results were obtained and shown in Fig. 6. The fitting curve was obtained by nonlinear fitting in Origin software. The saturation value of R_{tot} is ~3059 s^{-1} when the pump power is bigger than ~ 250 mW. Based on the tested data, the sensitivity coefficient K$_1$ and the maximum rotation rate Ω_{ym} under each pump powers were carried out and plotted in Fig. 7. The experimental results agree well with the theoretical prediction. The maximum sensitivity of 3818 (deg/s)$^{-1}$ is achieved under the optimized pump power of ~ 82 mW. The tested rotation response and the fitting curve under 82 mW were added in Fig. 4 and Table 1. As shown in Fig.7, the maximum rotation rate of ~ 21 deg/s is reached when pump power is bigger than 250 mW.

V. CONCLUSION

In summary, we developed a high linear atomic spin precession detection technique by modifying the fiber reflective Sagnac interferometer and operating it in closed-loop mode. The experimental setup of SERF gyro based on K-Rb-^{21}Ne comagnetometer with this detection module was built and its rotation response under different pump powers was tested experimentally. The tested results show that the gyro rotation response is nonlinear and the measurable dynamic range is limited. The cooperation condition of the self-compensating K-Rb-^{21}Ne co-magnetometer was analyzed and the nonlinear rotation response model was established by assuming the nuclei spin procession detecting as an *in-situ* magnetometer inside the SERF gyro. The model fitting curves agree well with the experimental results and confirm the assumption rationality. Furthermore, the optimized pump power for maximum sensitivity and measurable dynamic range of the SERF gyro were analyzed theoretically and demonstrated experimentally. And the curve of sensitivity and maximum measurable rotation rate were obtained with the proposed model. The investigation results indicate that the SERF gyro is propitious to a position gyroscope with high sensitivity.

REFERENCES

[1] H. C. Lefèvre, "The fiber-optic gyroscope: Achievement and perspective," *Gyroscopy Navigat.*, vol. 3, no. 4, pp. 223–226, Oct. 2012.

[2] V. M. N. Passaro, A. Cuccovillo, L. Vaiani, M. De Carlo, and C. E. Campanella, "Gyroscope technology and applications: A review in the industrial perspective," *Sensors*, vol. 17, no. 10, p. 2284, Oct. 2017.

[3] J. C. Fang and J. Qin, "Advances in atomic gyroscopes: A view from inertial navigation applications," *Sensors*, vol. 12, no. 5, pp. 6331–6346, May 2012.

[4] R. Li, W. Fan, L. Jiang, L. Duan, W. Quan, and J. Fang, "Rotation sensing using a K-Rb-^{21}Ne comagnetometer," *Phys. Rev. A, Gen. Phys.*, vol. 94, no. 3, Sep. 2016, Art. no. 032109.

[5] M. Larsen and D. Meyer, "Nuclear magnetic resonance gyro for inertial navigation," *Gyroscopy Navigat.*, vol. 5, no. 2, pp. 75–82, Apr. 2014.

[6] T. W. Kornack, R. K. Ghosh, and M. V. Romalis, "Nuclear spin gyroscope based on an atomic comagnetometer," *Appl. Phys. Lett.*, vol. 95, no. 23, Dec. 2005, Art. no. 230801.

[7] M. E. Limes, D. Sheng, and M. V. Romalis, "^{3}He–^{129}Xe Comagnetometery using ^{87}Rb detection and decoupling," *Phys. Rev. Lett.*, vol. 120, no. 3, Jan. 2018, Art. no. 033401.

[8] L. Jiang, W. Quan, R. Li, W. Fan, F. Liu, J. Qin, S. Wan, and J. Fang, "A parametrically modulated dual-axis atomic spin gyroscope," *Appl. Phys. Lett.*, vol. 112, no. 5, Jan. 2018, Art. no. 054103.

[9] S. J. Seltzer, "Developments in alkali-metal atomic magnetometry," Ph.D. dissertation, Princeton Univ., Princeton, NJ, USA, 2008, pp. 14 and 38–43.

[10] L. Xing, W. Quan, W. Fan, W. Zhang, Y. Fu, and T. Song, "The method for measuring the non-orthogonal angle of the magnetic field coils of a K-Rb-^{21}Ne co-magnetometer," *IEEE Access*, vol. 7, pp. 63892–63899, 2019.

[11] W. Fan, W. Quan, W. Zhang, L. Xing, and G. Liu, "Analysis on the magnetic field response for nuclear spin co-magnetometer operated in spin-exchange relaxation-free regime," *IEEE Access*, vol. 7, pp. 28574–28580, 2019.

[12] L. Duan, W. Quan, L. Jiang, W. Fan, M. Ding, Z. Hu, and J. Fang, "Common-mode noise reduction in an atomic spin gyroscope using optical differential detection," *Appl. Opt.*, vol. 56, no. 27, pp. 7734–7740, Sep. 2017.

[13] J. Fang, S. Wan, J. Qin, C. Zhang, W. Quan, H. Yuan, and H. Dong, "A novel Cs-^{129}Xe atomic spin gyroscope with closed-loop Faraday modulation," *Rev. Sci. Instrum.*, vol. 84, no. 8, Aug. 2013, Art. no. 083108.

[14] W. Quan, Q. Wang, and Y. Zhai, "A dual closed-loop drive and control system of photoelastic modulator for atomic magnetometer," *Meas. Sci. Technol.*, vol. 29, no. 6, May 2018, Art. no. 065105.

[15] H. Yao, Y. Li, D. Ma, J. Cai, J. Zhao, and M. Ding, "Acousto-optic modulation detection method in an all-optical K-Rb hybrid atomic magnetometer using uniform design method," *Opt. Express*, vol. 26, no. 22, pp. 28682–28692, Oct. 2018.

[16] X. Liu, Y. Yang, M. Ding, W. Quan, Y. Hu, Y. Li, W. Jin, and J. Fang, "Single-fiber Sagnac-like interferometer for optical rotation measurement in atomic spin precession detection," *J. Lightw. Technol.*, vol. 37, no. 4, pp. 1317–1324, Feb. 15, 2019.

[17] H. C. Lefèvre, *The Fiber-Optic Gyroscope*, 2nd ed. Norwood, MA, USA: Artech House, 2014, pp. 169–176.

[18] J. C. Fang and J. Qin, "*In situ* triaxial magnetic field compensation for the spin-exchange-relaxation-free atomic magnetometer," *Rev. Sci. Instrum.*, vol. 83, no. 10, Oct. 2012, Art. no. 103104.

[19] R. Li, W. Quan, W. Fan, L. Xing, and J. Fang, "Influence of magnetic fields on the bias stability of atomic gyroscope operated in spin-exchange relaxation-free regime," *Sens. Actuators A, Phys.*, vol. 266, pp. 130–134, Oct. 2017.

[20] L. Jiang, W. Quan, F. Liu, W. Fan, L. Xing, L. Duan, W. Liu, and J. Fang, "Closed-loop control of compensation point in the K-Rb-$_{21}$Ne comagnetometer," *Phys. Rev. Appl.*, vol. 12, no. 2, Aug. 2019, Art. no. 024017.

[21] J. Fang, R. Li, L. Duan, Y. Chen, and W. Quan, "Study of the operation temperature in the spin-exchange relaxation free magnetometer," *Rev. Sci. Instrum.*, vol. 86, no. 7, Jul. 2015, Art. no. 073116.

[22] Y. Chen, W. Quan, S. Zou, Y. Lu, L. Duan, Y. Li, H. Zhang, M. Ding, and J. Fang, "Spin exchange broadening of magnetic resonance lines in a high-sensitivity rotating K-Rb-^{21}Ne co-magnetometer," *Sci. Rep.*, vol. 6, Nov. 2016, Art. no. 36547.

YUANHONG YANG received the Ph.D. degree from Beihang University, Beijing, China, in 2004, where he is currently a Professor and a Ph.D. Supervisor with the School of Instrumentation and Optoelectronic Engineering. His research interests include optical fiber gyroscope, photoelectron devices, and distributed optical fiber sensing technology.

DONGYING CHEN received the B.S. degree in electrical engineering and automation from Shenli College, China University of Petroleum, China, in 2013, and the M.S. degree in instrument and meter engineering from Yanshan University, China, in 2016. She is currently pursuing the Ph.D. degree with the School of Instrumentation and Optoelectronic Engineering, Beihang University. Her research interests include the magnetic response of atomic magnetometer and comagnetometer operated in the spin-exchange relaxation free regime.

WEI JIN received the Ph.D. degree in optical fiber from Strathclyde University, U.K., in 1991. He is currently a Professor with the Department of Electrical Engineering, The Hong Kong Polytechnic University. His research interests include fiber sensing, photonic crystal fiber theory, fiber gas sensing technology, and fiber grating sensing technology.

WEI QUAN received the Ph.D. degree from Beihang University, in 2008, where he is currently a Professor with the School of Instrumentation and Optoelectronic Engineering. His research interests include celestial navigation and recently developed atomic inertial sensors based on alkali-metal vapor cell.

FENG LIU received the B.S. degree in control science and engineering from Shandong University, China, in 2014. He is currently pursuing the Ph.D. degree with the School of Instrumentation and Optoelectronic Engineering, Beihang University. His research interests include the magnetic response of atomic magnetometers and comagnetometer operated in the spin-exchange relaxation-free regime.

JIANCHENG FANG was born in Shandong, China, in 1965. He received the B.S. degree in electrical engineering from the Shandong University of Technology, Jinan, China, in 1983, the M.S. degree in automotive engineering from Xi'an Jiaotong University, Xi'an, China, in 1988, and the Ph.D. degree in mechanical engineering from Southeast University, Nanjing, China, in 1996. He is currently the Vice President of Beihang University, Beijing, China. He holds a special appointment professorship with the title of Cheung Kong Scholar, which was jointly established by the Ministry of Education of China and the Li Ka Shing Foundation. He has authored or coauthored over 150 articles and four books. His current research interests include attitude control system technology of spacecraft, novel inertial instrument and equipment technology, inertial navigation, and SERF atomic magnetometer and comagnetometer.

● ● ●